Geochemistry Geophysics Geosystems G3
AN ELECTRONIC JOURNAL OF THE EARTH SCIENCES
Published by AGU and the Geochemical Society

Article
Volume 1, Number 1
13 December 1999
1002, doi:10.1029/1999GC000003
ISSN: 1525-2027

Lateral mixing and advection of reactive isotopetracers in ocean basins: Numerical modeling

Heiner Igel

Institute of Theoretical Geophysics, Department of Earth Sciences, Downing Street, Cambridge CB2 3EQ, UK (igel@geophysik.uni-muenchen.de)

Now at Institut für Allgemeine und Angewandte Geophysik, Ludwig-Maximilians Universität Theresienstrasse 41, 80333 München, Germany

Friedhelm von Blanckenburg

Isotopengeologie, Universität Bern, Erlachstrasse 9a, CH-3012 Bern, Switzerland (fvb@mpi.unibe.ch)

[1] Ocean isotope tracers of intermediate residence time are becoming of increasing importance in studies of paleo-ocean circulation, global weathering fluxes, and trace pollutant dispersion in ocean basins. While analytical models exist that predict the way in which conservative tracers are dispersed in ocean gyres, the lateral movement of reactive tracers has not yet received much attention. Here we present time-dependent numerical simulations of the lateral mixing process (advection-diffusion-reaction) of reactive tracers with different residence times in gyres with varying Péclet number, diffusivity, western boundary intensification, and source geometry. Our main conclusions are that in our model gyre (1) homogenization of tracer concentrations and also of isotopic ratios in those cases where the isotopes have different pathways (e.g., atmospherically deposited cosmogenic ^{10}Be, continent-derived ^{9}Be) depends largely on the residence time and eddy diffusivity and isonly a weak function of Péclet number; (2) western intensification influences homogenization only in the case of short residence times and large Péclet numbers; (3) homogenization of isotopic ratios of continent-sourced tracers (e.g., ^{206}Pb/^{204}Pb, ^{143}Nd/^{144}Nd) is favored by high water velocities and hence shallow ocean levels; (4) boundary scavenging can result in significant lateral redistribution of output fluxes for even very short residence time tracers (e.g., ^{230}Th) if Péclet numbers are high; (5) the width of source and scavenging regions exerts a strong control over the actual tracer concentrations, but the spatial distribution and degree of tracer homogenization is not affected. The space dependence of input and scavenging is applicable to several reactive isotope tracers such as Be, Pb, Nd, Hf, Th, or Pa. Relative uniformity in their isotope ratios has been observed by mapping of these tracers in individual ocean basins (von Blanckenburg and Igel, 1999). Such uniformity would not be necessarily expected since the isotopes concerned enter through entirely different pathways. The simulations presented here demonstrate that homogenization of such short residence time tracers in ocean gyres is a feasible mechanism that can account for these observations.

Components: 10,402 words, 15 figures, 3 tables, 2 movies.

Keywords: Mixing in oceans; trace elements; boundary scavenging; beryllium; lead; isotope tracers; gyres.

Index Terms: 1050 Geochemistry: Marine geochemistry (4835, 4845, 4850); 3670 Mineralogy and Petrology: Minor and trace element composition; 4875 Oceanography: Biological and Chemical: Trace elements (0489); 4825 Oceanography: Biological and Chemical: Geochemistry.

source: https://doi.org/10.7892/boris.88518 | downloaded: 13.3.2024

Copyright 1999 by the American Geophysical Union

Received 21 May 1999; **Revised** 17 October 1999; **Accepted** 1 November 1999; **Published** 13 December 1999.

Igel, H., and F. von Blanckenburg (1999), Lateral mixing and advection of reactive isotopetracers in ocean basins: Numerical modeling, *Geochem. Geophys. Geosyst.*, *1*, 1002, doi:10.1029/1999GC000003.

1. Introduction

[2] Radiogenic and radioactive tracers extracted from oceanic sediments are being measured with continually improving levels of analytical sophistication, the results of which are being utilized in paleoceanography to help understand the history of ocean circulation and climate change [*Yu et al.*, 1996; *Ling et al.*, 1997; *Christensen et al.*, 1997]. The currently available means of measuring extremely low levels of reactive trace elements dissolved in seawater allow us to map the extent to which these elements are dispersed in the oceans and provide insights into their relative riverine, hydrothermal, aeolian, or anthropogenic sources [*Schaule and Patterson*, 1981; *Measures et al.*, 1984; *Helmers and Rutgers van der Loeff*, 1993; *Bruland et al.*, 1994; *Hamelin et al.*, 1997]. Depending on the particular tracer being considered, the mechanisms and locations of transfer into the oceans can be very different. Some areinput through weathering and erosion of continents (e.g., stable Pb, rare earth element (REE), Al, ^{9}Be), some are of cosmogenic origin (e.g., ^{10}Be, ^{14}C) and are deposited from the atmosphere,and some are produced in the water column by in situ decay of U (^{230}Th, ^{231}Pa, ^{210}Pb). The input in the two latter cases is spatially more uniform. Despite these varying sources, observations of isotope concentrations and ratios reveal a high degree of homogenization in oceanic basins [*Piepgras and Wasserburg*, 1980; *Albarède and Goldstein*, 1992; *Abouchami and Goldstein*, 1995; *von Blanckenburg et al.*, 1996a, 1996b]. Furthermore, evidence from isotopic measurements of dissolved Pb in seawater has shown that pollutant Pb can be transported to great distances from its continental sources [*Schaule and Patterson*, 1981; *Flegal et al.*, 1986; *Hamelin et al.*, 1997]. These observations pose the question of the relevant transport processes. Several mechanisms for the mixing of reactive tracers are possible. These are (1) homogenization at the source, (2) interbasin exchange, and (3) lateral intrabasin dispersion through advection in subtropical gyres and eddy mixing. The feasibility of these different mechanisms are extensively discussed in the work of *von Blanckenburg and Igel* [1999]. They argue that for some of the reactive tracers, mechanisms 1 and 2 can be ruled out or are likely to contribute only marginally to the homogenization. Therefore mechanism 3 seems the most likely to explain the observed distributions.

[3] Mixing of conservative (nonreactive, passive) tracers in oceanic gyres has been studied in the past [e.g., *Rhines and Young*, 1983; *Young*, 1984; *Musgrave*, 1985; *Pickart*, 1988; *Figueroa*, 1994; *Richards et al.*, 1995; *Hecht et al.*, 1995], but the effects of space-dependent scavenging on the homogenization of reactive tracers in gyres has had little attention to date. In order to investigate the efficiency of mixing of reactive tracers in a simple model gyre we perform numerical calculations and study the steady state concentrations observed for various advection reaction schemes. The space dependence of tracer input and the range of gyre velocities and residence times are applicable to several reactive tracers at various depth levels, since both the scavenging intensity of tracers and also water velocity are dominant functions of water depth. While we are aware of the limitations of our highly simplified gyre model, this is a first step to quantify the trends of the various contributing factors such as Péclet number (thus the relative effects of velocity of the gyre circulation relative to eddy diffusivity), western boundary intensification (asymmetry in the velocity field), residence time (tracer reactivity, scavenging), diffusivity, and source geometry, which allows us to discuss the feasibility of intrabasin mixing in comparison to other potential mechanisms.

[4] After introducing the physical model and description of our model gyre we will present several examples of time-dependent and steady state solutions for various parameter combinations. Mixing efficiency will be discussed by comparing the final standard deviation normalized by the mean concentration as a function of the variables mentioned above. The aim here is neither to investigate accurate analytical solutions to tracer patterns as those that have been derived for passive tracers [e.g., *Rhines and Young*, 1983; *Young*, 1984; *Musgrave*, 1985; *Pickart*, 1988; *Figueroa*, 1994; *Richards et al.*, 1995; *Hecht et al.*, 1995] nor to present predictive tools for reactive tracer patterns

that depend on a large number of variables [e.g., *Henderson et al.*, 1999]. Rather, we assess the feasibility of processes that lead to the observed good homogenization of reactive tracers [*von Blanckenburg and Igel*, 1999] and in particular the effect of such mixing on isotope ratios, which are becoming an increasingly important aspect of paleoceanography.

2. Description of the Model

2.1. Theory and Numerical Method

[5] Our physical system can be described with the two-dimensional time-dependent advection-diffusion-reaction equation [e.g., *Boudreaux*, 1997]:

$$\partial_t C = k(\partial_x^2 + \partial_y^2)C - (v_x\partial_x + v_y\partial y)C - RC + p, \qquad (1)$$

where C is the tracer concentration, k is the (constant) eddy diffusivity, v_x and v_y are the components of the velocity field, R is the removal rate (the inverse of the residence time τ, and p is the input term. The ∂_t denotes partial differentiation with respect to time (or space with subscripts x and y). Time and space dependence are implicit.

[6] We solve (1) numerically employing the upwind-staggered finite difference scheme suggested by *Smolarkiewicz* [1983] for the advection term and follow the approach by *Pickart* [1988] for the diffusion term. The time extrapolation is carried out by a second-order Taylor expansion. A careful comparison of different advection schemes was carried out by *Hecht et al.* [1995], which demonstrated the accuracy of the algorithm used in our study. Our numerical method has been successfully verified against the test solutions by *Smolarkiewicz* [1983] for advection and against analytical solutions to the diffusion equation for steady state problems. The implementation is, in principle, equivalent to the scheme by *Pickart* [1988] with the exception of boundary conditions. Since we are interested in studying mixing in a closed system, our boundary conditions impose no flux and no diffusion across all boundaries by setting the normal gradient of the concentration to zero. As we assess the feasibility of certain mixing phenomena rather than providing accurate predictions, we have ignored all three-dimensional effects, including those of seafloor topography. This is an approach commonly used in two-dimensional gyre studies for tracer mixing [e.g., *Rhines and Young*, 1983; *Young*, 1984; *Musgrave*, 1985; *Pickart*, 1988; *Richards et al.*, 1995].

2.2. Gyre Geometry, Advection, and Eddy Mixing

[7] Our model gyre has a domain width of 8000 km and is discretized on a 200 × 200 grid. This implies a space increment of 40 km. The velocity field is described by the *Stommel* [1948] circulation scheme, the main parameter being ε, the relative width of the western boundary current. Gyres with narrow western boundary currents are usually observed in nature. To assess a lower limit of cross-streamline flux, in our study we use either a symmetric gyre (ε = 1) or a gyre with relative boundary width (ε = 0.2) unless otherwise stated. The corresponding stream function and the velocity field of those two model gyres are shown in Figure 1. The circulation is clockwise.

2.3. Geometry of Input and Scavenging

[8] The velocities of the gyre are scaled according to a given Péclet number Pe following the approach by *Richards et al.* [1995]. The stream function is normalized such as to have a maximum value of ψ_{max} = Pe k, where k is the diffusivity. In all simulations the diffusivity is kept constant at 16,000 km^2/a (~5 × 10^{-6} cm^2/s), except in the section below where the effects of diffusivity on the final steady state are discussed. This is a reasonable mean value for eddy diffusivity which is not a strong function of depth [*Ku and Luo*., 1994].

[9] The spatial source distribution depends on the particular tracer to be modeled. We model two different source functions for the tracers. One describes all tracers entering the ocean basins from the continents by erosion. This continental input (CI) describes tracers entering the oceans at point sources by river dissolved or river particulate matter (e.g., ^{9}Be, Nd, stable Pb) is described by two bell-shaped Gauss functions on both sides of the gyre (Figure 2, left) with a half width 500 km in all simulations except in section 3.3 where the effect of changing source the half width is evaluated. The center of the Gauss functions is 500 km away from the boundaries. The source input p is constant with time $p(x,y,t) = p(x,y)$ with p_{max} = 1 [1/yr]. The other input is uniform (UI)(e.g., cosmogenic ^{10}Be, ^{14}C, ^{230}Th, or ^{231}Pa from U to in situ decay), and is describedby a constant across the whole gyre $p(x,y)$ = 1 [1/yr]. The space-dependent removal (scavenging) is also described by Gauss functions. The stronger scavenging observed at the gyre boundaries is accounted for by centering two Gauss functions at the same

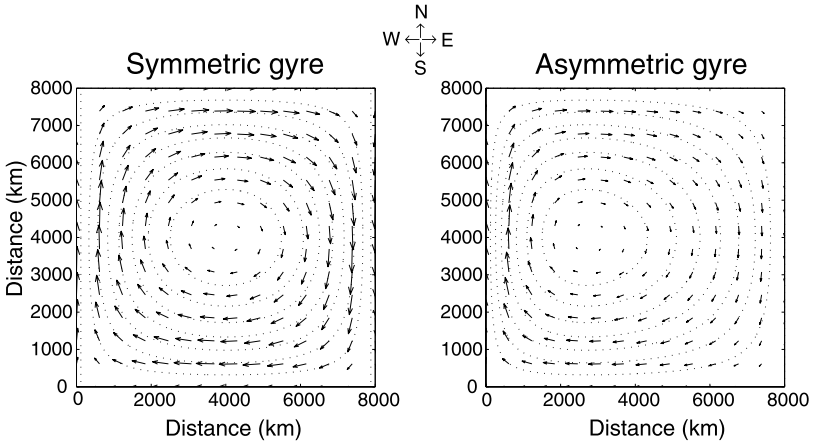

Figure 1. Stream function (dotted lines) and velocity fields (arrows) for the advection schemes used in our simulations. (left) Symmetric Stommel gyre ($\varepsilon = 1$). (right) Western intensification ($\varepsilon = 0.2$). The velocity fields are scaled according to the Péclet number (see text for details).

locations as the input but with increased half width of 1000 km. An example is shown in Figure 2 (right). In section 3.3 the effect of changing the scavenging half widths is explored. Throughout the paper we describe the scavenging by the maximum tracer residence time τ_{max}, which is the residence time in the interior gyre. The removal rate R in (1) is the inverse of the residence time τ. In all simulations the residence time inside the gyre is 10 times larger than the maximum residence time at the center of the high scavenging boundary regions, which is in accordance with observations [*Anderson et al.*, 1990; *Lao et al.*, 1992]. In Figure 2 (right) most of the gyre is described by a residence time of 100 years, but in the strong scavenging regions the residence time decreases to a minimum of 10 years.

[10] Certainly, this physical model for oceanic advection and reaction of tracers is highly simplified. However, in order to understand the basic effects of input and scavenging we chose to keep the model as simple as possible. Further effects on the final steady state solutions can be expected from a number of causes, including (1) interbasin mixing associated with the global thermohaline circulation, (2) cross-gyre flux and mixing through equatorial countercurrents, (3) time-dependent advection, (4) stress-dependent diffusivity, (5) vertical tracer interaction, and (6) time-dependent

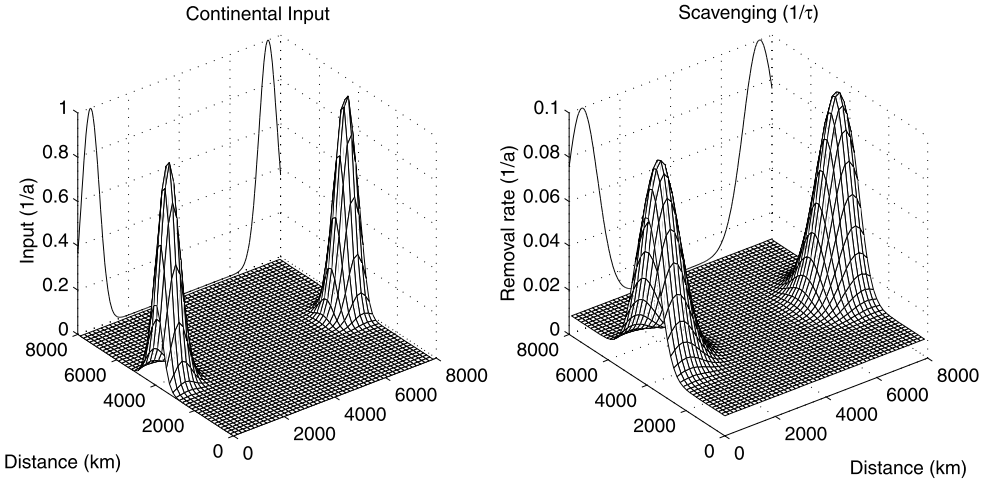

Figure 2. (left) Spatial dependence of the tracer input for continental input (CI). The eastern and western inputs are described by Gauss functions with 500 km half width. The E-W cross section is shown along the northern boundary. (right) Spatial dependence of the removal rate (the inverse of the residence time) in our model gyre. The boundary scavenging is described by two Gauss functions with half width 1000 km. Inside the gyre the residence times are 10 times longer than the minimum residence time near the boundaries.

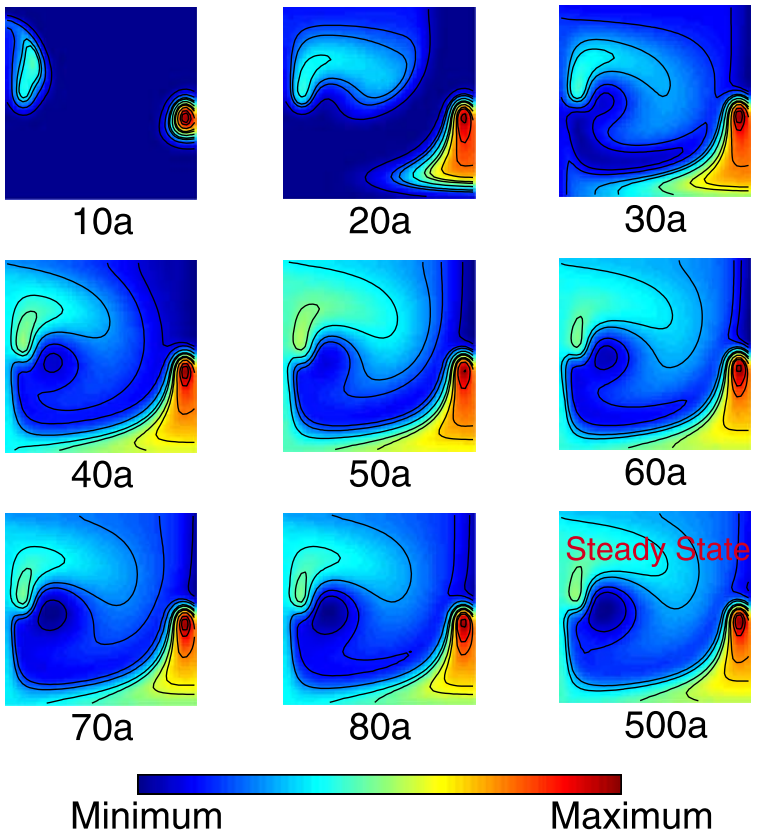

Figure 3. Snapshots of CI tracer concentration at different times. Contour lines, equally spaced between minimum and maximum, are superimposed. In this simulation the Péclet number is 100, and the maximum residence time is 100 years. This leads to a gyre with an average velocity of 440 km/yr and a maximum velocity near the western boundary of 2700 km/yr. The circulation is asymmetric ($\varepsilon = 0.1$). The domain width is 8000 km. The snapshot shown in the bottom right corner is the final steady state concentration. Snapshots of tracer concentration are shown every 10 years. Owing to the higher northward velocities at the western boundary the advection away from the source region is more effective there. The slower velocities at the eastern boundary lead to a maximum in tracer concentration developing slightly south of the maximum eastern source input. Furthermore, because the two sources are not centered on the same streamlines (as in the symmetric case) tracers from the western source are advected into the more internal parts of the gyre. Also, tracers emitted by the western source can escape the high scavenging zones more easily. At short residence times this improves homogenization.

input and scavenging. When observations will allow constraints on these mechanisms, they can easily be included into the numerical modeling scheme, for example, in combination with global circulation models (GCM) [e.g., *Henderson et al.*, 1999].

3. Mixing of Uniform and Continental Input

3.1. Time Evolution of Model Gyre for Continental Input and Mixing Times

[11] An example of the time evolution of the tracer concentration for an asymmetric gyre with $\varepsilon = 0.1$ is shown in Figure 3, and in two animations for continental input and uniform input (Movies 1 and 2). The main characteristics of the final steady state concentration in terms of space dependence are reached at an early stage (e.g., 50 years) but because of the continuous input and removal the standard deviation σ_m with respect to the mean concentration still evolves. In this paper we will describe the mixing efficiency by this measure of the degree of tracer homogenization σ_m, the standard deviation relative to the mean value. Note that the steady state σ_m for isotopic ratios is independent of the rate of input of the individual isotopes, or the isotopic ratios of the left- and right-sourced tracers. In other words, $\sigma_m(c_1/c_2) = \sigma_m[(ac/_1)/(bc_2)]$, where $c_{1,2}$ are the final concentrations of two isotopes in the system and a,b are arbitrary positive numbers.

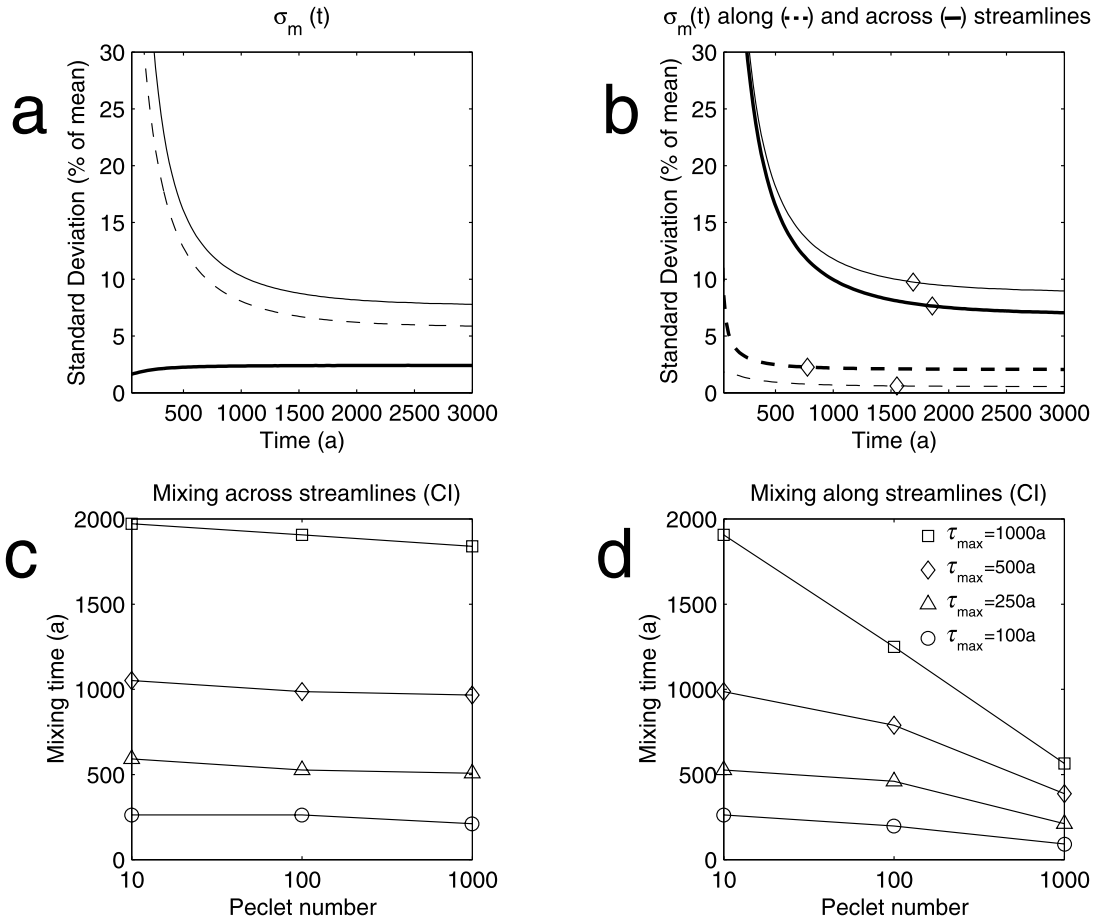

Figure 4. (a) Standard deviation (with respect to the mean concentration) as a function of time for continental input, uniform input and their ratio for Pe = 300, and τ_{max} = 1000 years. The standard deviation σ_m for CI decreases rapidly at the beginning of the simulations and is within 10% of its final value after one (maximum) residence time τ_{max} (1000 years in this example). The σ_m value for UI increases with time due to the homogeneous input, which is turned increasingly heterogeneous by the space-dependent scavenging. The time evolution of σ_m for the ratio (UI/CI) is basically following the CI case but is increased over CI because of the entirely different spatial distribution patterns of the two tracers. (b) Same setup as in Figure 4a but showing the evolution of the standard deviation σ_m along (dashed) and across (solid line) streamlines. σ_m across streamlines decreases slowly with time as CI needs to diffuse into the interior, which is a slow process. In contrast, σ_m along streamlines decreases rapidly, because advective mixing at the prescribed Pe of 300 is rapid. Mixing times (defined here as the time at which σ_m is 10% above the steady state σ_m) are also shown by the open diamond symbols. At large Péclet numbers these times are much shorter for mixing along streamlines than across streamlines. (c) Mixing times for CI tracers as defined in Figure 4b for homogenization across streamlines as function of Pe for various residence times as shown in Figure 4d. Mixing times across streamlines are principally a function of residence time (Figure 4c) and are virtually independent of Péclet number. This is because mixing across streamlines requires diffusion of tracer into the interior, which is limited only by scavenging and hence residence time. In our definition of mixing time, a longer residence time allows for more and better homogenization, and as a result, the 10% σ_m above the steady state σ_m is reached later the longer the residence time. In our model gyre these mixing times are roughly twice the residence time τ_{max}. (d) Mixing times along streamlines. Mixing times along streamlines are a strong function of Péclet number (Figure 4d). This originates from the increased stirring with high Pe which reduces heterogeneity along streamlines and results in a much more rapid approach to the final steady state standard deviation.

[12] An example of the time-dependence of σ_m for CI and UI as well as their ratio are shown in Figure 4a. The standard deviation σ_m for CI decreases rapidly at the beginning of the simulations and is within 10% of its final value after one (maximum) residence time τ_{max}. In order to ensure that the system has reached the steady state all simulations are carried out for five maximum residence times.

[13] In a further step, we evaluate the time evolution of σ_m for CI and the UI/CI ratio along and

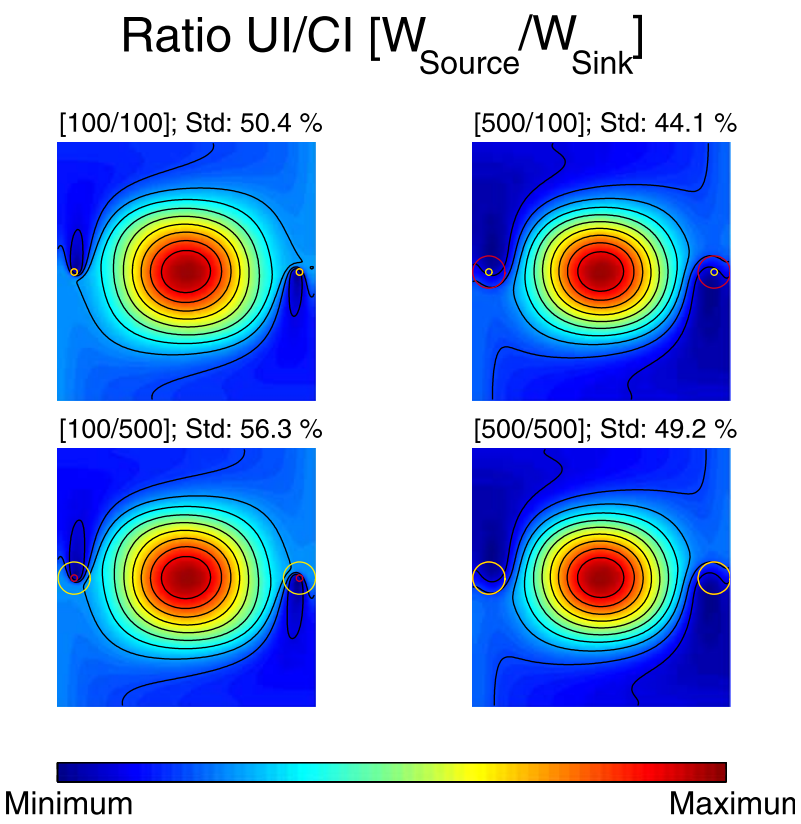

Figure 5. Steady state UI/CI ratio and resulting standard deviation σ_m for different source half widths and sink half widths [W_{source}/W_{sink}]. Simulations have been performed with Pe = 50 and τ_{max} = 100 years. In this setting the effect of varying source and sink half widths should show most sensitively as the low Pe and short residence times ensure that CI tracers, after emerging from their source, are not removed too rapidly from the source and sink area. Source and sink half width are indicated by red and yellow lines, respectively. Contour lines, equally spaced between minimum and maximum, are superimposed. Note that varying half widths have virtually no effect on the spatial distribution patterns. The tracer concentrations, however, are strongly affected (not shown). The exploration of σ_m in a larger parameter space is summarized in Tables 1a–1c.

across streamlines (Figure 4b). The σ_m value across streamlines decreases slowly with time as CI needs to diffuse into the interior, which is a slow process. In contrast, σ_m along streamlines decreases rapidly, because advective mixing at the prescribed Pe of 300 is rapid. Mixing times are also shown. While *Richards et al.* [1995] have calculated mixing time as the time at which σ_m reaches 10% of the overall concentration, such definition is not possible if scavenging is involved. We have defined a mixing time here as the time at which σ_m is 10% above the steady state σ_m. At large Péclet numbers these times are much shorter for mixing along streamlines than across streamlines (Figure 4b). Of interest is a general comparison of mixing times across and along streamlines for various residence times and Pe numbers. This comparison is presented for a continental input tracer in Figures 4c and 4d. Mixing times across streamlines are principally a function of residence time (Figure 4c) and are virtually independent of Péclet number. Mixing times along streamlines are a strong function of Péclet number (Figure 4d).

[14] Below we will investigate the effects of source and sink geometry, maximum residence time τ_{max}, Péclet number Pe, western intensification ε, and diffusivity k on the final steady state σ_m for CI, UI, and their ratio. Several simulations were undertaken with the aim of exploring a wide range of the model space. First, individual simulation results will be presented showing the trends, and finally σ_m as a function of the various parameters will be discussed.

3.2. Source and Sink Half Width

[15] *Young* [1984] and *Richards et al.* [1995] have shown that tracer distributions are sensitive to the

Table 1a. Standard Deviations as a Function of Source and Sink Half Width for Continental Input CI

		Pe = 50		Pe = 200	
		W_{source} (km)		W_{source} (km)	
τ_{max} (y)	W_{sink} (km)	100	500	100	500
100	100	41%	34%	37%	31%
	500	42%	33%	38%	30%
500	100	12%	10%	11%	10%
	500	12%	10%	11%	9%

Table 1c. Standard Deviations as a Function of Source and Sink Half Width for Ratio CI/UI

		Pe = 50		Pe = 200	
		W_{source} (km)		W_{source} (km)	
τ_{max} (y)	W_{sink} (km)	100	500	100	500
100	100	50%	44%	52%	45%
	500	56%	49%	59%	50%
500	100	12%	11%	12%	10%
	500	14%	12%	14%	12%

way in which tracers are introduced into the gyre. We have evaluated this effect by varying both the source half width (W_{source}) and the sink half width (W_{sink}) between 100 and 500 km for Péclet numbers of 50 and 200, and open-ocean residence times τ_{max} of 100 and 500 years. As shown by *Richards et al.* [1995], there is a strong effect on actual tracer concentrations and UI/CI ratios. In general, mean UI concentrations are reduced by increasing W_{sink}, whereas mean CI concentrations increase strongly with increase in W_{source}. Similarly, the UI/CI ratio is reduced strongly by an increase in W_{source}.

[16] In this study the spatial distribution patterns of tracers and their description by relative standard deviations σ_m are of more concern than the actual concentrations. In Figure 5 the distributions of UI/CI ratio are shown for various source and sink half widths. Changing half widths results in very small changes of spatial distribution, with only modifying W_{source} resulting in a small change in σ_m of the UI/CI ratio. Standard deviations of CI, UI, and their ratio as a function of source and sink half width are summarized in Tables 1a–1c. The principle observations are the following: CI standard deviations are reduced by wider W_{source} for short residence times, are virtually independent of Pe, and are relatively insensitive to both W_{source} and W_{sink} at longer residence times. UI standard deviations are reduced by a factor of ~4 at τ_{max} of 100 years by reducing W_{sink}, but this variation is only a factor of ca. 2 at τ_{max} of ~500 years. The standard deviation of the UI/CI ratio is, in general, insensitive to changes in both W_{source} and W_{sink}.

Table 1b. Standard Deviations as a Function of Source and Sink Half Width for Uniform Input UI

		Pe = 50	Pe = 200
τ_{max} (y)	W_{sink} (km)	σ	σ
100	100	1.4%	1.6%
	500	6.2%	5.8%
500	100	1.4%	1.6%
	500	2.3%	2.4%

3.3. Residence Time and Péclet Number

[17] The final steady state concentration after five maximum residence times are shown in Figure 6 for CI, UI, and their ratio. The principle observations are the space-dependent distributions of the final CI and UI concentrations are almost the inverse of each other, because the CI input is space dependent, whereas the initially uniform UI is scavenged at the same locations. Local heterogeneities remain in the low-velocity regime (Pe = 15), while these heterogeneities are smoothed along streamlines in the high-velocity regime (Pe = 300). The overall ranges, and hence standard deviations σ_m in CI, UI concentrations, and UI/CI isotope ratios, are similar in both the high- and low-velocity regime. An increase in the residence time τ_{max}, however, increases the concentrations and reduces σ_m for CI, UI, and their ratio considerably.

3.4. Western Boundary Intensification

[18] To investigate the effects of western boundary intensification (WBI) on the mixing, we simulate a Stommel gyre with $\varepsilon = 1$ (Figure 7a), and $\varepsilon = 0.2$ (Figure 7b). Pe = 100 and τ_{max} = 100 years. Homogenization is much better in the case of a strong western boundary current. As noted already by *Young* [1984], this feature is due to the fact that a strong WBI has a similar effect as increasing the diffusivity: cross-streamline mixing is easier with narrow streamlines; also, tracers input into narrow boundaries are advected more readily into the interior gyre from narrow boundary currents.

3.5. Horizontal Eddy Diffusivity

[19] Estimates for the horizontal eddy diffusivity k in the oceans vary over an order of magnitude. In

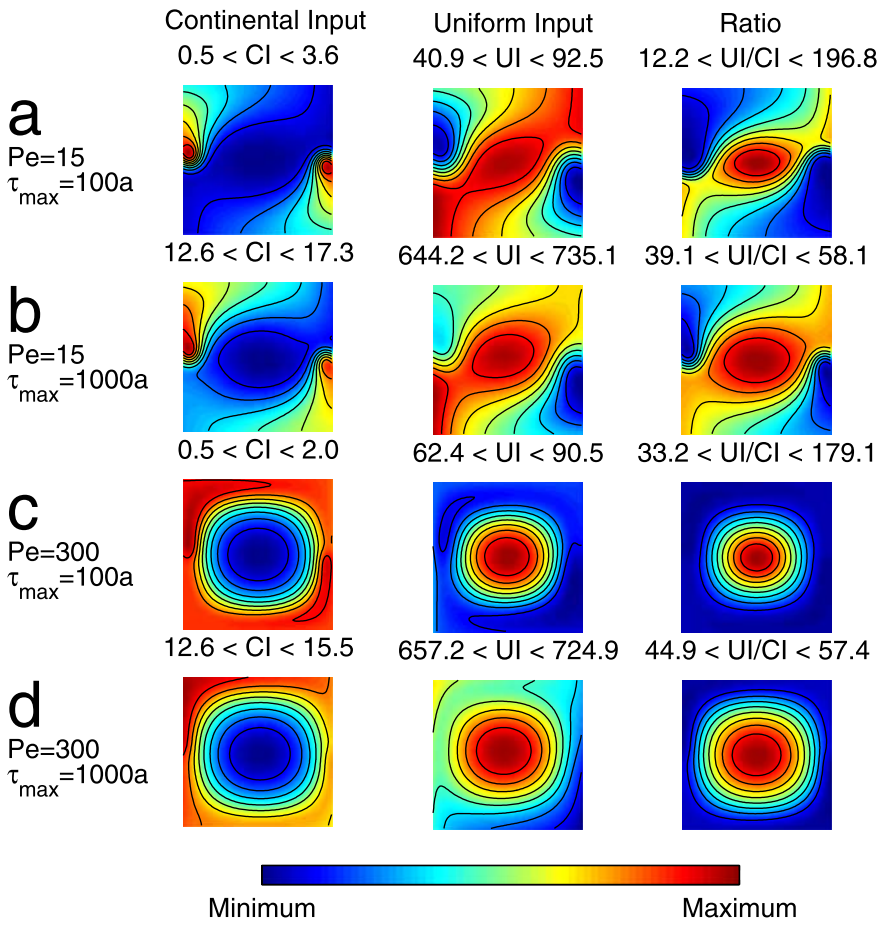

Figure 6. The final steady state concentration after five maximum residence times for (left) continental input (CI), (middle) uniform input (UI), and (right) their ratio (UI/CI). Simulations are a symmetric gyre (Figure 1, left). Minima and maxima values of tracer concentration (or their ratio) are given above each graph. Contour lines, equally spaced between minimum and maximum, are superimposed. (a) Pe = 15 (the mean and maximum velocities in the symmetric gyre are 69 and 154 km/yr, respectively); τ_{max} = 100 years. The space-dependent distributions of the final CI and UI concentrations are almost the inverse of each other. The CI concentration is high near the sources and decreases along the streamlines around the gyre. The UI concentration is minimal in the zones of strong removal which coincide with the regions of strong CI. Note that these minima and maxima are not in the same location as the maxima of input and scavenging, but they are (slightly) shifted downstream. The heterogeneity of input and scavenging leads to considerable variations in concentration across the gyre in the steady state. The final relative standard deviations are 56, 17, and 57% for CI, UI, and their ratio (always UI/CI), respectively. (b) Pe = 15, τ_{max} = 1000 years; all other parameters have been kept constant. The space dependence looks very similar to the previous case, the final concentrations and thus the relative standard deviations have changed considerably. Note that the heterogeneities in the input and scavenging regions are less pronounced. The final σ_m are 9, 7, and 12% for CI, UI, and their ratio, respectively. The longer residence time of the tracers has allowed much enhanced homogenization. (c) Pe = 300 (mean velocity of 1390 km/yr and a maximum velocity of 3090 km/yr), τ_{max} = 100 years. The effects of stronger advection are studied by fixing the maximum residence time to 100 years and setting Pe = 300. This was done by changing the velocity while keeping k constant at 16,000 km^2/yr ($\sim 5 \times 10^6$cm^2/s).The strong advection has almost completely removed the input and scavenging generated heterogeneity along the near-boundary streamlines seen in the previous examples. Inside the gyre the concentration isolines follow almost exactly the streamlines, implying near-perfect mixing along the flow direction. The final UI/CI ratio shows almost no sign of the boundary heterogeneities observed for low Pe apart from the gradient into the center of the gyre. The final standard deviations σ_m are 33, 10, and 34% for CI, UI, and their ratio, respectively. In comparison with the simulation shown in Figures 6a and 6b (Pe = 15) one can note that although the homogenization has improved along the streamlines, the final standard deviation is still large compared to the case where the residence time was increased. (d) Pe = 300, τ_{max} = 1000 years. Strong advection is combined with long residence times. The final steady state concentrations and ratio are almost constant along the streamlines. The final σ_m are 5.8, 2.5, and 7.9% for CI, UI, and their ratio.

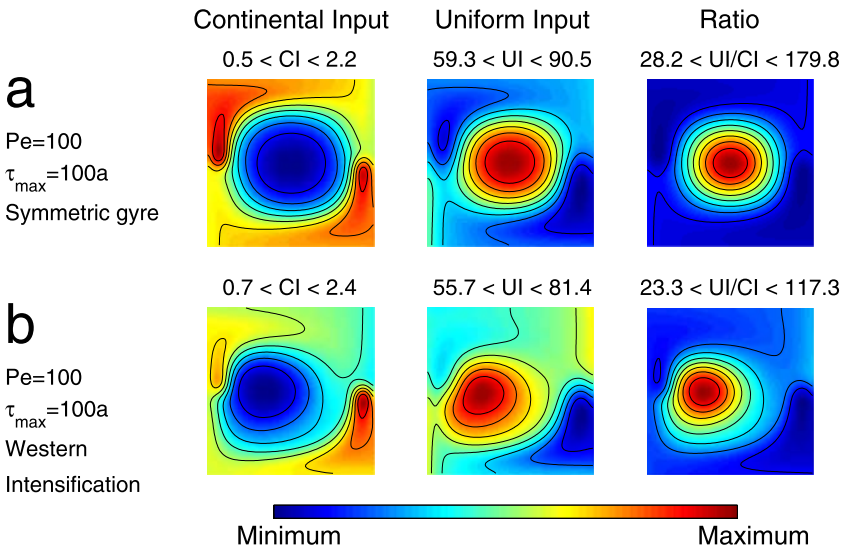

Figure 7. To investigate the effects of western boundary intensification (WBI) on the mixing we simulate a (a) symmetric gyre ($\varepsilon = 1$), and with (b) western intensification ($\varepsilon = 0.2$). Pe = 100 and τ_{max} = 100 years. Steady state tracer concentration and ratio are shown for (left) continental input (CI), (middle) uniform input (UI), and (right) their ratio (UI/CI). Minima and maxima are given above each graph. Contour lines, equally spaced between minimum and maximum, are superimposed. (a) The results for a Strommel gyre with $\varepsilon = 1$. The mean and maximum velocities in the symmetric gyre shown are 460 and 1030 km/yr, respectively. The final standard deviations are 33, 11, and 58 for CI, UI, and their ratio. (b) The results for a Stommel gyre with $\varepsilon = 0.2$. At Pe = 100 this gyre has mean and maximum velocities of 440 and 1700 km/yr, respectively. Compared to the symmetric gyre the mean velocities are approximately the same, but the maximum velocity is considerably larger, having its maximum in the western boundary zone. Because the differences in velocities in the input and strong scavenging region are much higher than elsewhere, there are stronger gradients along the near-boundary streamlines than in the symmetric case. The region with small velocities has maximum (CI) or minimum (UI) concentration. The final standard deviations with WBI are 24, 8, and 39% for CI, UI, and their ratio. Thus homogenization is considerably improved in the asymmetric gyre with WBI.

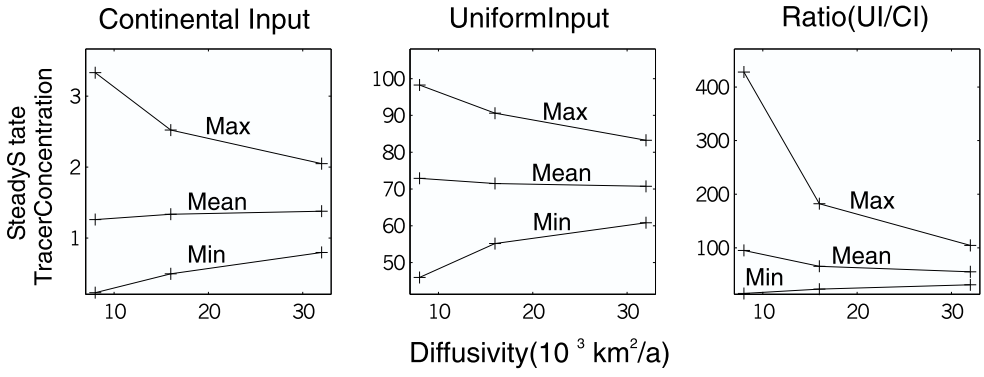

Figure 8. The dependence of the steady state concentrations on diffusivity. Three simulations were carried out for k = 8000, 16,000, and 32,000 km^2/yr (~2.5, 5, and 10 × 10^6 cm^2/s). In all simulations, v_{mean} = 240 km/yr (Pe = 50 for k = 8000 km^2/yr); τ_{max} = 100 years. The maxima, minima, and mean values of steady state tracer concentration are shown for (left) continental input, (middle) uniform input, and (right) their ratio as a function of diffusivity. While the space dependence and the mean of the final concentrations are almost independent of diffusivity, the range of concentrations and thus the standard deviation is strongly influenced by it. The final standard deviations for these runs were 61, 40, and 25% (CI); 19, 12, and 8% (UI); and 95, 60, and 35% for their ratio (UI/CI) for the diffusivities mentioned above, respectively. The range (and thus the standard deviation) decreases with increasing diffusivity.

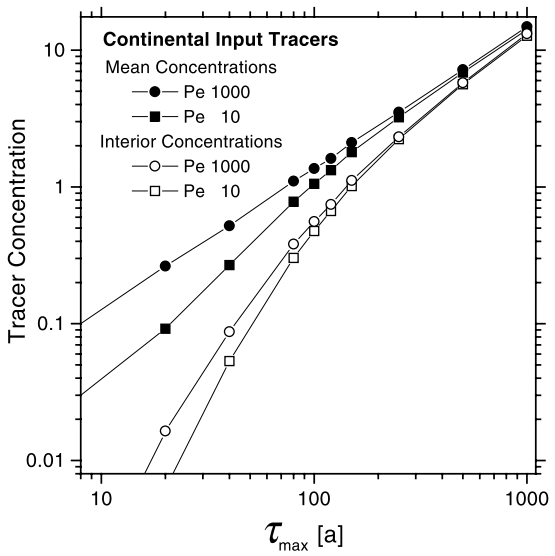

Figure 9. Mean CI tracer concentrations and concentrations in the interior 2000 × 2000 km as a function of residence time τ_{max} and two bounding Péclet numbers (k = 16,000 km^2/yr). The interior concentrations give an indication of the actual tracer amounts that can escape the margin areas. Runs are for symmetric geometry. Mean concentrations are a near-linear function of residence time (in log-log scale). At higher velocities (Péclet numbers), tracers are removed more effectively from the high-scavenging zones, thereby increasing concentrations. Differences between interior concentrations and mean concentrations are large at short residence times, but this difference decreases as the residence time increases. This is expected as residence time exerts the primary control over homogenization.

Figure 8 we show results from simulations with diffusivity k = 8000, 16,000, and 32,000 km^2/yr (~2.5, 5, and 10 × 10^{-6} cm^2/s), respectively. While the space dependence and the mean of the final concentrations are almost independent of diffusivity, the range of concentrations and thus the standard deviation is strongly reduced with increasing diffusivity. The effects of changing diffusivity are more pronounced for CI and the ratio because the diffusion term in (1) depends on the second space derivatives and thus have stronger effects in the more heterogeneous CI model.

3.6. CI Tracer Concentrations in the Interior Gyre

[20] In the previous section we have shown that under certain conditions efficient tracer dispersion from the near-continent sources into the interior gyre can take place, thereby reducing heterogeneity. In Figure 9 we show a summary of mean concentrations in the entire gyre, and also minimum concentrations which would be found in the interior 2000 km of the gyre. At higher velocities (Péclet numbers), tracers are removed more effectively from the high-scavenging zones, thereby increasing concentrations. Higher residence times also increase interior concentrations. Most importantly, the minimal concentrations are an indicator of how much tracer can be transferred from the boundaries to the interiors. At residence times shorter than 10 years virtually no tracer escapes from the margins. At τ_{max} of 20-40 years the tracer concentration found in the interior is larger than 5–10% of the mean concentration; at 80 years this is already about half of the mean concentration.

3.7. Homogenization of CI, UI, and Their Ratio

[21] To investigate the dependence of the steady state relative standard deviation as a function of the parameters described above, several simulations were undertaken. We show the combined results as standard deviation in percent of the mean final concentration in steady state for all simulations in Figure 10.

[22] For moderate Péclet numbers, σ_m for CI decreases as a function of Pe (Figure 10a). For high Péclet numbers the degree of homogenization does not depend on the mean velocity of the gyre. For reasons explained above, western intensification has a marked effect at shorter residence times but much less effect at longer residence times. For high Pe and short residence times a stronger western boundary current improves the homogenization. The final standard deviation in all CI cases depends strongly on the residence time. The same general observations hold for the UI models shown in Figure 10b, with the main difference of smaller absolute values of σ_m because of the homogeneity of the input. The standard deviations of the UI/CI ratio for all parameters are shown in Figure 10c. There is less dependence on the Péclet number compared with the individual isotopes.Mixing of the UI/CI ratio depends dominantly on the residence time of the isotopes and at high Pe also on whether a strong western boundary current is present.

4. Modeling Mixed Tracer Continental Input

4.1. Mixed Isotope Sources

[23] We now investigate a different input scavenging system applicable, for example, to isotopes

such as continental-sourced Pb, Nd, or Hf. We restrict ourselves to simulating a symmetric gyre as shown in Figure 1(left). The space dependence of the scavenging is the same as in the previous simulations (Figure 2, right). One of the tracers (from now on denoted as t_1) is input with equal rates (1/yr) from both the eastern and the western sources, while the other (denoted as t_2) is different for the eastern (1.5/yr) and western (0.5/yr) source. This ratio remains fixed for all simulations and is meant to represent input of a tracer with an arbitrarily fixed isotopic ratio of 1.5 (east) and 0.5 (west). This could be the ratio of a radiogenic to a primordial stable isotope (e.g., $^{206}Pb/^{204}Pb$). The spatial source functions are illustrated in Figure 11.

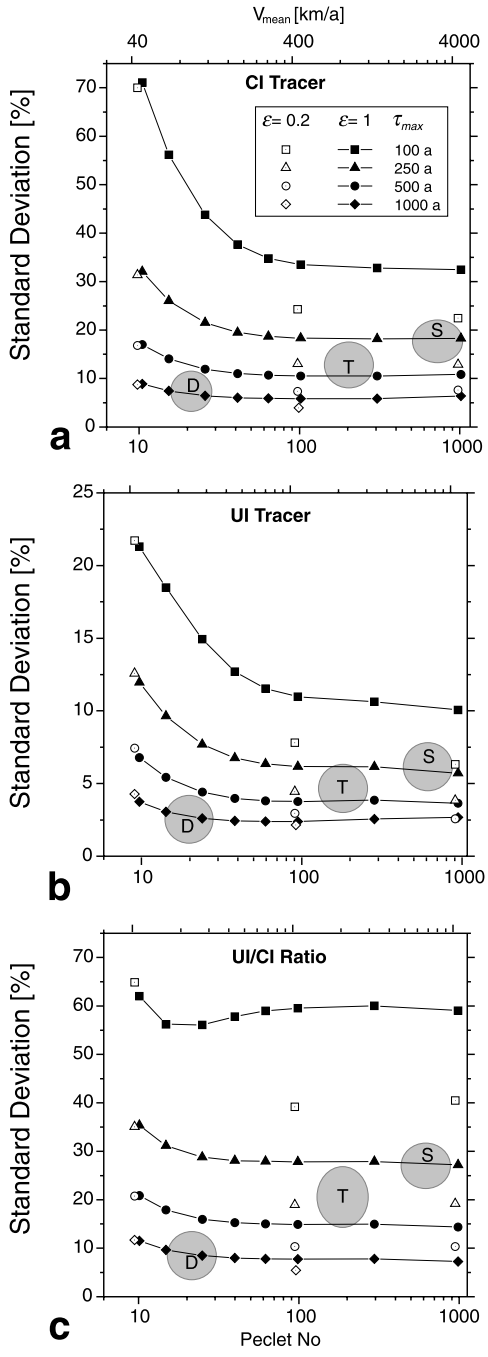

Figure 10. Several simulations were undertaken to investigate the dependence of the steady state relative standard deviation as a function of the parameters described above. The Péclet number varied from Pe = 10 to Pe = 1000, with average velocities ranging from 46 to 4600 km/yr, respectively. The maximum residence times were allowed to vary from 100 to 1000 years. The only other setup that changed was the symmetry of the gyre as described above. The horizontal eddy diffusivity was held constant at a mean ocean value of 16,000 km^2/yr. (a) Standard deviation for CI, (b) standard deviation for UI, (c) standard deviation of UI/CI ratio as a function of Péclet number (mean velocity). Grey areas are examples for water velocities typical for various depth levels [*Semtner and Chervin*, 1992] and maximum open ocean residence timesfor Be [*von Blanckenburg et al.*, 1996b], where the observed deep water residence time was scaled relative to dissolved concentrations at shallower levels). S, surface; T, thermocline; D, deep water. In reality, tracer standard deviations will follow certain trajectories governed by a combination of lateral mixing and vertical tracer transfer in the water column. These paths have been explained by *von Blanckenburg and Igel* [1999]. (a) For moderate Péclet numbers σ_m for CI decreases as a function of Pe (or mean velocity). For high Péclet numbers the degree of homogenization does not depend on the mean velocity of the gyre. Western intensification has a marked effect at small residence times but much less effect at longer residence times. For high Pe and short residence times a stronger western boundary current improves the homogenization. The final standard deviation in all CI cases depends strongly on the residence time. (b) The same general observations hold for the UI models shown, with the main difference of smaller absolute values of σ_m because of the homogeneity of the input. (c) For the standard deviations of the UI/CI ratio, there is less dependence on the Péclet number compared with the individual isotopes. Mixing of the UI/CI ratio depends dominantly on the residence time of the isotopes and at high Pe also on whether a strong western boundary current is present.

4.2. Péclet Number and Residence Time

[24] Because one of the motivations for these simulations is to provide insight into the mechanism by which the relatively homogeneous Pb isotope distributions in the Pacific basin comes about [*von Blanckenburg and Igel*, 1999], residence times τ_{max} the following simulations were held in the range of Pb (2–150 years). Accordingly, they are shorter than those of the CI-UI models. In the first example the maximum residence time is

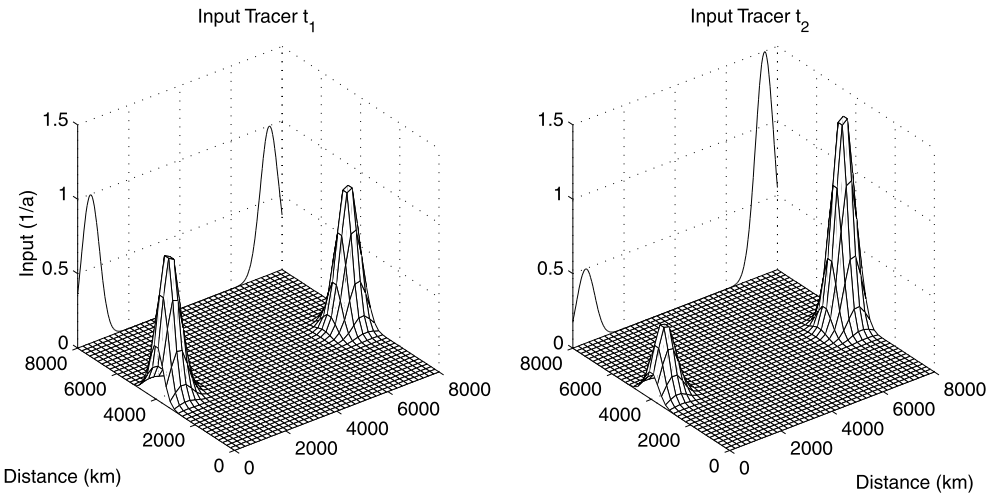

Figure 11. Space dependence of input for mixed source simulations. Half width of the Gauss functions is 500 km. (left) Input tracer t_1, equal amounts from both sources. (right) Input tracer t_2, different amounts from both sources.

2 years in the center of the gyre for a variety of Pe numbers (Figure 12). Complex isotope distribution patterns result, which are in some cases completely decoupled from the source points. Overall, there is very little homogenization.

[25] For the same circulation scheme as in Figure 12a (Pe = 10) but a maximum residence time of 150 years, conditions more akin to Pb in deep water, homogenization is more efficient (Figure 13a). Advection is now able to carry an isotopic ratio to the opposite sides of the gyre. It is interesting to note, however, that these gradients develop in anorth-south direction, although the differences in input are east-west aligned.

[26] Near-perfect isotopic ratio homogenization is attained when Pe = 1000 is combined with τ_{max} = 150 years (Figure 13b). Isotopic ratio heterogeneities resulting from the different source inputs are almost completely smoothed out by mixing along streamlines, and in the isotopic ratio, only some fine structure remains with a final standard deviation of only 0.3%, the concentrations attain a much higher final standard deviation of 28% (t_1) and 32% (t_2).

[27] The results on both tracer concentration and tracer isotope ratios of mixed sources are summarized in Figure 14. While the homogenization of tracer concentrations improves with both residence time and Péclet number (Figure 14a), homogenization of isotope ratios are best at high Péclet numbers (Figure 14b). This is because isotopes are mixed along the outermost streamlines, such that the tracers that are available for slow diffusion into the interior consist already of a well-homogenized isotope blend.

5. Discussion

5.1. Mixing of Continental and Uniform Input

[28] The following results can be derived from the individual tracer concentration simulations from either continental or uniform input:

[29] 1. The final standard deviation σ_m of concentrations depends on the Péclet number for small Pe values (e.g., Pe < 100). For larger Pe, homogenization is not improved by stronger advection, and a finite homogenization σ_m is attained at a characteristic Pe that is higher the shorter the residence time. At this characteristic Pe, homogenization along streamlines is at its maximum for a given residence time, increasing advective mixing would not lead to any further improvement. This phenomenon can also be viewed to be equivalent to systems with input (CI) and/or scavenging (UI) at all boundaries. In this case the local imprints of the input locations would have been lost.

[30] 2. While tracer concentrations are sensitive to the half width of the source (CI) and to the half width of the sink (UI), the spatial distribution patterns of tracers and their ratios as characterized by their standard deviation are relatively insensitive to the geometry of source and scavenging regions.

[31] 3. Homogenization is improved at short residence times for a gyre with the same mean velocity

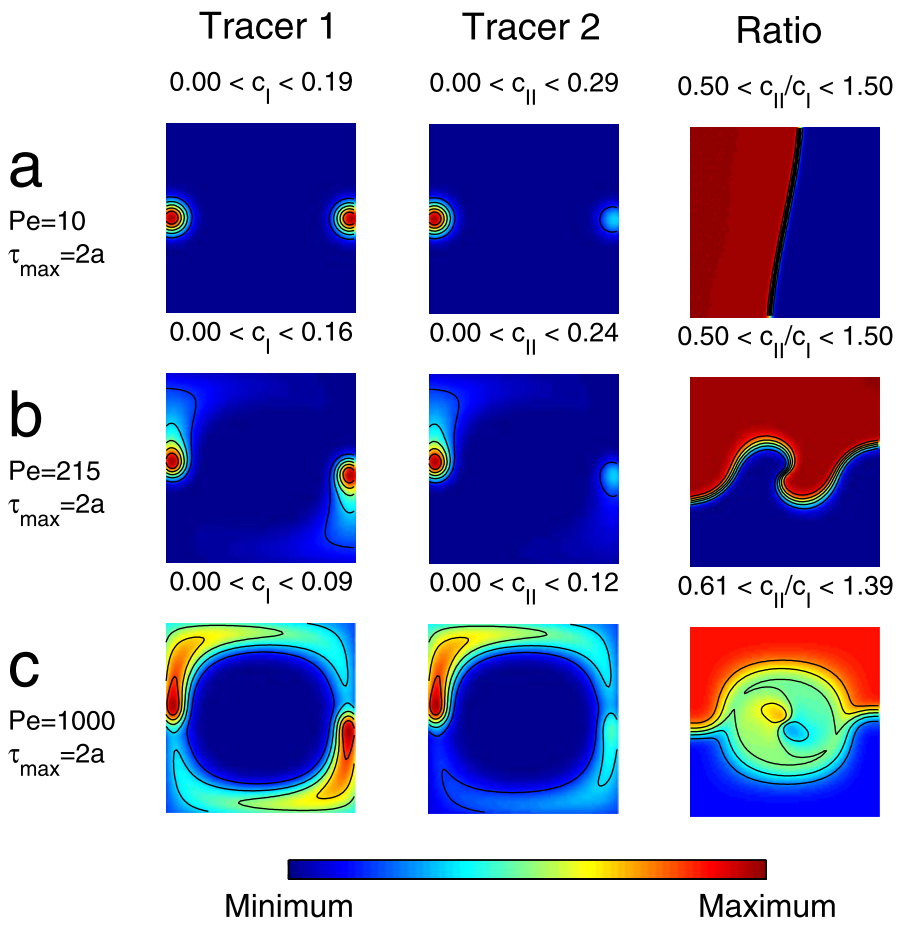

Figure 12. Experiments simulating the input of Pb, Nd, or Hf with mixed isotope ratios for τ_{max} = 2 years. This ratio remains fixed for all simulations and represents input of a tracer with an arbitrarily fixed isotopic ratio of 1.5 (east) and 0.5 (west). Steady state tracer concentration and ratio for continental input from tracer (left) t_1, (middle) t_2, and (right) their ratio (t_2/t_1) for a symmetric gyre (Figure 1, left). Minima and maxima values are given above each graph. White corresponds to the maximum concentration and black to minimum concentration. Contour lines, equally spaced between minimum and maximum, are superimposed. (a) The maximum residence time is 2 years in the center of the gyre. The Péclet number Pe = 10 with an average velocity of 46 km/yr. Owing to the short residence time and the small velocities only a very small fraction of the mixtures is able to leave the source region. Therefore there is a strong E-W gradient of the ratio. (b) Increasing the Péclet number to 215 while τ_{max} = 2 years results in an average velocity of 990 km/yr and the maximum velocity in the source region of 2200 km/yr. Advection is now strong enough to transport the mixtures away from the source regions. Near the center of the gyre a type of fingering occurs. The mixtures from both sources seem to spiral around the center of the gyre while they are obstructed at the eastern and western boundaries. The reason is that in the center of the gyre the residence times are 10 times longer than in the strong scavenging regions on both sides (see Figure 1, right). Therefore, even though the velocities are small near the center of the gyre, owing to the longer residence time the mixtures are advected around the gyre near its center leading to heterogeneities in the cross sections through the center of the ratios (Figure 12b, right). The final standard deviation for the ratio is 48%, thus almost no mixing occurred. In this setup, 50% standard deviation corresponds to the absence of any homogenization. (c) Pe = 1000 with mean velocity 4600 km/yr and maximum velocity 10,000 km/yr while τ_{max} = 2 years as in the previous simulations. These velocities would by typical of surface water. Because of the much longer residence times inside the gyre, fingering occurs leading to the heterogeneities for the isotope ratios seen in the center of the gyre, while the individual absolute tracer concentrations are very small. The final standard deviation is 30%.

and residence times but western intensification (WBI). For long residence times (>500 years) the final σ_m is only slightly affected. This is because WBI has the same effect as increasing the eddy diffusivity: enhancing the cross-streamline flux. At long residence times, eddy diffusion dominates over this effect. WBI does not influence mixing at low Pe, because advective transport is too small

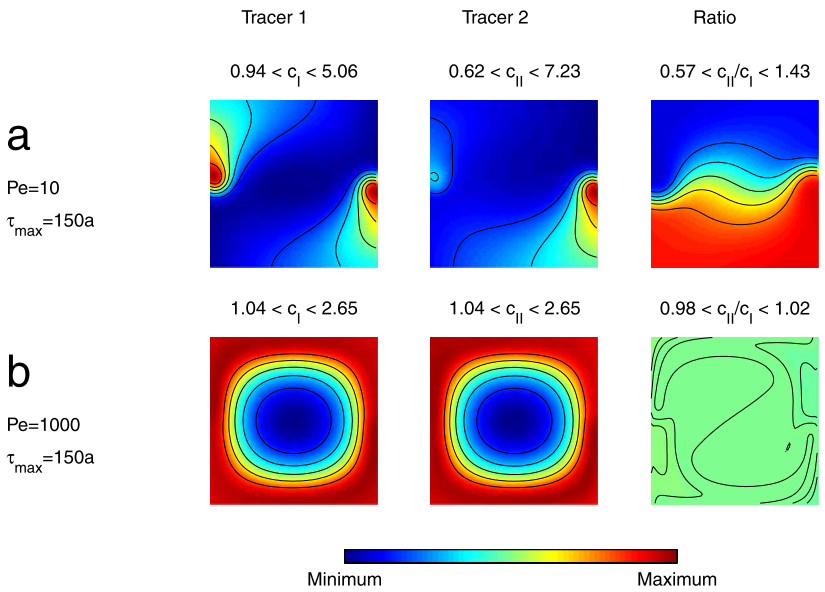

Figure 13. Steady state tracer concentration and ratio for continental input from tracer (left) t_1, (middle) t_2, and (right) their ratio (t_2/t_1) for a symmetric gyre (Figure 1, left) for τ_{max} = 150 years. These residence times are akin to those of Pb in deep water. Minima and maxima values are given above each graph. (a) Pe = 10, τ_{max} = 150 years. Homogenization is more efficient than in the low-τ case (Figure 12). Advection is now able to carry an isotopic ratio to the opposite sides of the gyre. Because of the low velocities strong gradients of the ratio persist. It is interesting to note, however, that these gradients develop in a north-south direction, although the differences in input are east-west aligned. (b) Pe = 1000, τ_{max} = 150 years. Near-perfect isotopic ratio homogenization is attained. The contour lines of the final concentrations are almost identical to the streamlines, but strong concentration gradients remain perpendicular to streamlines. This is expected because cross-streamline mixing is by tracer diffusion of which the extent is limited by scavenging. Hence, although isotopic ratio heterogeneities resulting from the different source inputs are almost completely smoothed out and in the isotopic ratio only some fine structure remains with a final standard deviation of only 0.3%, the concentrations attain a much higher final standard deviation of 28% (t_1) and 32% (t_2).

to have a significant effect regardless of the geometry.

[32] 4. Homogenization for all Péclet numbers depends strongly on the residence times. Longer residence times lead to better mixing. This is because scavenging effectively counterbalances slow diffusive homogenization, which is required for moving tracers from their sources into the interior gyre. This is also evident from the mixing times (the time required for the tracer to reach the final steady state standard deviation) which is independent of Pe number for mixing across streamlines and is higher the longer the residence time.

[33] 5. Changing the horizontal eddy diffusivity has almost no effect on the space dependence and the mean of steady state tracer concentration, but the final σ_m is smaller for increased diffusivity. Diffusivity smoothens the final tracer distributions in regions of strong gradients thereby reducing σ_m.

[34] 6. The relative amounts of CI tracer transferred from the boundaries into the interior gyre is a function of residence time in the case of the symmetric gyre. If τ_{max} is greater than 20 years, appreciable amounts of tracer can arrive in the central gyre.

[35] For the ratio of uniform to continental input the same observations hold with one exception:

[36] The UI/CI ratio is almost independent of Pe for moderate to high Pe. The explanation for this phenomenon is that regardless of the degree of advective homogenization, which mainly acts to remove boundary heterogeneities and produces homogenous concentrations along streamlines, the actual spatial distributions of CI and UI remain almost accurate inverse images of each other. Then to form the ratio UI/CI, for example, a high UI concentration is always divided by a low CI concentration and vice versa, resulting in a large range of ratios and hence a large standard deviation. To reduce ratio heterogeneity, diffusive smoothing of the inverse distribution is necessary. As noted above, this is favored by long residence times.

[37] As a practical example, typical ranges for Be scavenging residence times and water velocities as a function of depth are shown by the gray areas in Figures 10a-10c. In this case, cosmogenic ^{10}Be would be represented by UI, and continental-sourced ^{9}Be by CI. These show that a relative standard deviation in ^{10}Be/^{9}Be of 10-20% can be achieved with our model gyre in deep water and in the thermocline but that also surface waters can reduce the heterogeneity to 30%. In practice, tracer homogenization will be governed by incremental steps of lateral mixing followed by transfer of tracers into a deeper level. These trajectories have been explained by *von Blanckenburg and Igel* [1999].

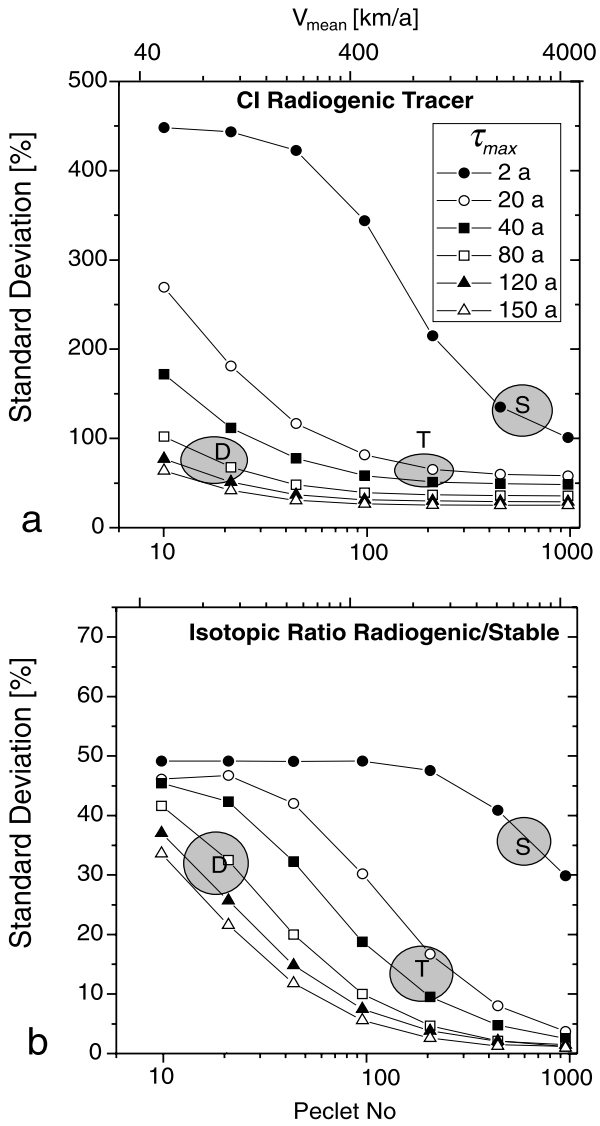

5.2. Homogenization of Mixed Sources

[38] The simulations for mixed sources have been carried out for shorter residence times to be compatible with the Pb isotope observations. The results shown in Figure 14 show that for a tracer input at both sides, small Péclet number and short residence time almost no homogenization occurs. This is not surprising as the tracers are hardly escaping the strong scavenging input region. In principle, the same observations (1–5) mentioned above hold for these simulations. However, the isotope ratio (Figure 14b) shows dependence of σ_m on Pe even for large Péclet numbers. For short residence time (2 years) and low Péclet number (Pe < 300), basically no homogenization occurs because the tracers are unable to escape the input region. For longer residence times, homogenization of the ratio of the tracers depends strongly on Pe and hardly on residence time.With strong advection, homogenization is almost perfect for long residence times. The tracer sources are located within the outermost streamlines, which ensures rapid mixing of these tracers immediately as they enter the oceans. Inward diffusion of these CI tracers, required to homogenize concentration, will have no significant effect on isotopic ratio homogenization as advective mixing along streamlines has produced an already highly homogenized blend.

Figure 14. Standard deviation for the mixed source simulations for (a) tracer t_2 (input as Figure 10, right) and (b) ratio t_2/t_1 as a function Péclet number (mean velocity). For a tracer input at both sides, small Péclet number, and short residence time, almost no homogenization occurs (Figure 14a). This is because tracers are hardly escaping the strong scavenging input region. However, the isotope ratio (Figure 14b) shows dependence of σ_m on Pe even for large Péclet numbers. For short residence time (2 years) and low Péclet number (Pe < 300), basically no isotope homogenization occurs because the tracers are unable to escape the input region. For longer residence times, homogenization of the isotope ratio of the tracers strongly depends on Pe and hardly on residence time. Inward diffusion of these CI tracers, required to homogenize concentration, will have no significant effect on isotopic ratio homogenization as advective mixing along streamlines has produced an already highly homogenized blend. The gray areas are examples for dissolved Pb at velocities typical for various depth levels [*Semtner and Chervin*, 1992] and residence times (2 years in surface water, 20–40 years in thermocline water, 80 years in deep water [*Schaule and Patterson*, 1981]).

[39] The gray areas (Figure 14) show typical Pb residence times and velocities for different vertical sections in the oceans. Homogenization is most efficient in thermocline waters. In the thermocline water, velocities are high, while τ is 20–40 years [*Schaule and Patterson*, 1981], a model standard deviation of ±10% can be achieved, similar to that observed in nature [*von Blanckenburg and Igel*, 1999]. Better homogenization in both concentration and isotopic composition is expected for the case of dissolved Nd, because its residence time is much higher (~2000 years).

5.3. Boundary Scavenging and Deposition for Uniform Input

[40] Boundary scavenging is the process that results in deposition of particle-reactive chemical tracers in ocean margin sediments at a much greater rate than their average rate of deposition over the interior ocean [*Bacon*, 1988]. In our model we have implicitly incorporated boundary scavenging by a tenfold increase of the tracers removal rate in boundary regions over that of the rest of the basin (Figure 2). In Figure 15 we illustrate controls on the tracer depositional flux in an east-west section through the gyre. The tracer input is uniform over the entire basin area as shown by the straight solid line. High residence times (τ_{max} = 1000 years; e.g., ^{10}Be, Figure 15a) favor transport of tracers from the interiors to the high scavenging zones. This transport results in a deficit of deposition in the interiors, and a sevenfold increase of deposition over production at the margins. Such patterns were qualitatively predicted for ^{10}Be [*Anderson et al.*, 1990], and also observed in Holocene sediments [*Lao et al.*, 1992]. The integrated rate of deposition in the east-west section is higher than production. This is because tracers are advected into the boundary zones from areas located further to the north or south. For long τ, such behavior is similar for all Péclet numbers (Figure 15a). Figure 15b shows a case of intermediate residence time (τ_{max} = 100 years; e.g., ^{231}Pa, ^{210}Pb). The overall pattern is similar to that of τ_{max} = 1000 years, but the deficitin the interior is smaller; also, the boundary deposition is reduced at low Péclet numbers. At short residence times (τ_{max} = 10a; e.g., ^{230}Th, Figure 15c) the magnitude of depositional flux is a strong function of Péclet number. Although for such short τ transport length scales are commonly assumed to be limited and hence the depositionalflux is expected to be more or less uniform, the patterns shownin Figure 15c show that this is the case only for a low-velocity

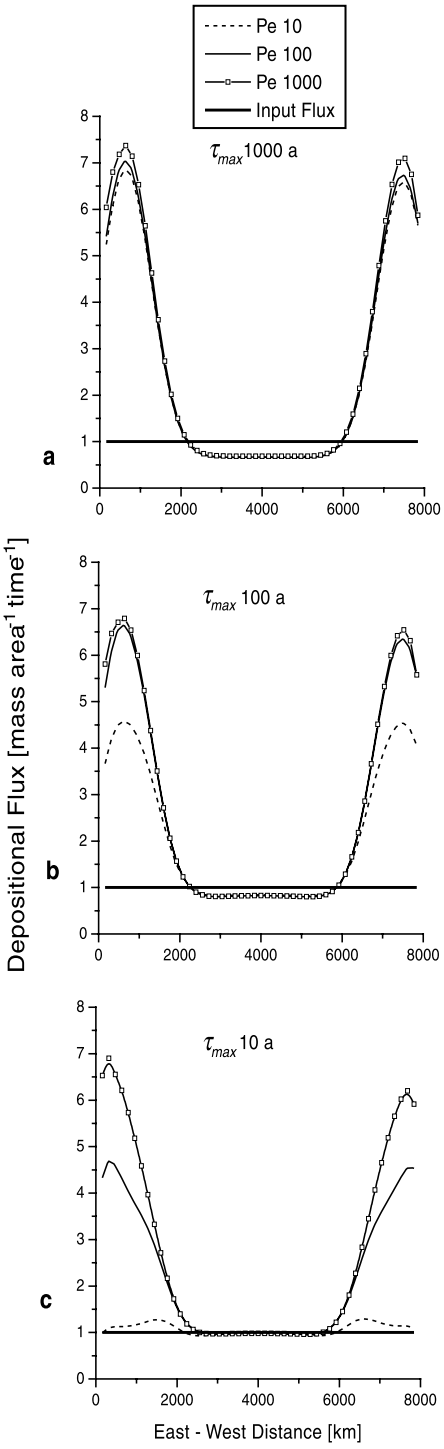

Figure 15. Depositional flux for UI tracers for various Pe and residence times along an east-west section through the gyre. The marginal sites of high depositional flux are those of enhanced scavenging. The thick solid line shows the input flux (1/yr).

regime. At higher Péclet numbers, deposition shows a strong pattern of boundary scavenging which is similar to that of Pa or Be.

[41] These model results have implications for the procedure by which depositional fluxes of longer τ tracers are derived from their concentrations in the sediment by normalizing them to the flux of ^{230}Th, which is assumed to be constant [*Lao et al.*, 1992]. *Henderson et al.* [1999] have demonstrated that this assumption is not necessarily valid in all areas of the oceans and have calculated in a global circulation model a potential excess in ^{230}Th deposition over production of a factor of 1.6 is possible. Our simulation shown in Figure 15c demonstrates a possible sevenfold excess in ^{230}Th deposition over production for the high Péclet number regime.While the overall magnitude of ^{230}Th boundary scavenging will not be as large as in our strongly advective regime, because most of the ^{230}Th is produced by in situ U decay deep in the water column where Péclet numbers are low, the case demonstrated, nevertheless, confirms that this procedure can result in serious underestimation of these inferred fluxes in boundaryzones with strongly advective regimes.

6. Conclusions

[42] Our results suggest that homogenization of tracer concentrations and also of isotopic ratios of uniform input (e.g., ^{10}Be) to continental input (e.g., ^{9}Be) in our model gyre depends mainly on the residence times of these tracers. For nutrient-type elements the residence time is greatest at depth. Observations on the lateral and vertical distribution of Be isotopes show that the ^{10}Be/^{9}Be ratio is most poorly homogenized at the surface and best homogenizedat depth [*von Blanckenburg and Igel*, 1999], which is in accordance with these predictions. Isotopic ratio homogenization of tracers with continental point sources depends mainly on water velocity. Because water velocities are high in surface and thermocline waters circulating gyres will contribute considerably to isotopic homogenization of natural or pollution Pb. Homogenization will improve successively if these tracers are transferred to depth, for example, by reversible exchange with sinking particles. In contrast, isotopic tracers that are injected locally into deep water, for example, by import from other ocean basins through the thermohaline circulation, will generate isotope distributions that are much less homogenized owing to low advection than they would be if these tracers were injected near surface. Observations from Nd isotopes in Pacific Antarctic Bottom Water, for example, are distinct from surrounding water masses [*Albarède and Goldstein*, 1992]. Continent-sourced tracers can reach the interiors of large gyres if their open-ocean residence time is at least 20 years. As this is even the case for some of the most reactive elements in thermocline water, there is a feasible pathway for enriching the interior oceans in trace metals even if other pathways (eolian sources, hydrothermal fluids) are not available.The importance of these results lies in the fact that we now have a framework within which these different pathways may be identified from oceanographic observations.

Acknowledgments

[43] We gratefully acknowledge the High Performance Computing Center in the Earth Sciences at the Institute of Theoretical Geophysics, Cambridge, for providing access to their computational facilities. The comments by Brian Dade, Harry Elderfield, Thomas Stocker, Adam Schultz and the reviews of three anonymous referees were very helpful.

References

Abouchami, W., and S. L. Goldstein (1995), A lead isotopic study of Circum–Antarctic manganese nodules, *Geochim. Cosmochim. Acta*, *59*, 1809–1820.

Albarède, F., and S. L. Goldstein (1992), World map of Nd isotopes in sea-floor ferromanganese deposits, *Geology*, *20*, 761–763.

Anderson, R. F., Y. Lao, W. S. Broecker, S. E. Trumbore, H. J. Hofmann, and W. Wölfli (1990), Boundary scavenging in the Pacific Ocean: A comparison of ^{10}Be and ^{231}Pa, *Earth Planet. Sci. Lett.*, *96*, 287–304.

Bacon, M. P. (1988), Tracers of chemical scavenging in the ocean: Boundary effects and large-scale chemical fractionation, *Philos. Trans. R. Soc. London, Ser. A*, *325*, 147–160.

Bruland, K. W., K. J. Orians, and J. P. Cowen (1994), Reactive trace metals in the stratified central North Pacific, *Geochim. Cosmochim. Acta*, *58*, 3171–3182.

Boudreau, B. P. (1997), *Diagenetic Models and Their Implementation*, 414 pp., Springer-Verlag, New York.

Christensen, J. N., A. N. Halliday, L. V. Godfrey, J. R. Hein, and D. K. Rea (1997), Climate and ocean dynamics and the lead isotopic records in Pacific ferromanganese crusts, *Science*, *277*, 913–918.

Figueroa, H. A. (1994), Eddy resolution versus eddy diffusion in a double gyre GCM, part II, Mixing of passive tracers, *J. Phys. Oceanogr.*, *24*, 387–402.

Flegal, A. R., K. Itoh, C. C. Patterson, and C. S. Wong (1986), Vertical profile of lead isotopic compositions in the northeast Pacific, *Nature*, *321*, 689–690.

Hamelin, B., J. L. Ferrand, L. Alleman, E. Nicolas, and A. Veron (1997), Isotopic evidence of pollutant lead transport from North America to the subtropical North Atlantic gyre, *Geochim. Cosmochim. Acta*, *61*, 4423–4428.

Hecht, M. W., W. R. Holland, and P. J. Rasch (1995), Upwind-weighted advection schemes for ocean tracer transport: An evaluation in a passive tracer context, *J. Geophys. Res.*, *100*, 20,763–20,778.

Helmers, E., and M. M. Rutgers van der Loeff (1993), Lead and aluminium in Atlantic surface waters (50°N to 50°S) reflecting anthropogenic and natural sources in the eolian transport, *J. Geophys. Res.*, *98*, 20,261–20,273.

Henderson, G. M., C. Heinze, R. F. Anderson, and A. M. E. Winguth (1999), Global distribution of the ^{230}Th flux to ocean sediments constrained by GCM modelling, *Deep Sea Res.*, *46*, 1861–1893.

Ku, T.L., and S. Luo (1994), New appraisal of radium 226 as a large-scale oceanic mixing tracer, *J. Geophys. Res.*, *99*, 10,225–10,273.

Lao, Y., R. F. Anderson, W. S. Broecker, S. E. Trumbore, H. J. Hofmann, and W. Wölfli (1992), Transport and burial rates of ^{10}Be and ^{231}Pa in the Pacific Ocean during the Holocene period, *Earth Planet. Sci. Lett.*, *113*, 173–189.

Ling, H. F., K. W. Burton, R. K. O'Nions, B. S. Kamber, F. von Blanckenburg, A. J. Gibb, and J. R. Hein (1997), Evolution of Nd and Pb isotopes in Central Pacific seawater from ferromanganese crusts, *Earth Planet. Sci. Lett.*, *146*, 1–12.

Measures, C. I., B. Grant, M. Khadem, D. S. Lee, and J. M. Edmond (1984), Distribution of Be, Al, Se, and Bi in the surface waters of the western North Atlantic and Caribbean, *Earth Planet. Sci. Lett.*, *71*, 1–12.

Musgrave, D. L. (1985), A numerical study of the roles of subgyre-scale mixing and the western boundary current on homogenization of a passive tracer, *J. Geophys. Res.*, *90*, 7073–7043.

Pickart, R.S. (1988), Entrainment and homogenization of a passive tracer in a numerical model gyre, *J. Geophys. Res.*, *93*, 6761–6773.

Piepgras, D. J., and G. J. Wasserburg (1980), Neodymium isotopic variations in seawater, *Earth Planet. Sci. Lett.*, *50*, 128–138.

Rhines, P. P., and W. R. Young (1983), How rapidly is a passive scalar mixed within closed streamlines, *J. Fluid Mech.*, *133*, 133–145.

Richards, K. J., Y. Jia, and C. F. Rogers (1995), Dispersion of tracers by ocean gyres, *J. Phys. Oceanogr.*, *25*, 873–887.

Schaule, B. K., and C. C. Patterson (1981), Lead concentrations in the northeast Pacific: Evidence for global anthropogenic perturbations, *Earth Planet. Sci. Lett.*, *54*, 97–116.

Semtner, A. J., Jr., and R. M. Chervin (1992), Ocean general circulation from a global eddy-resolving model, *J. Geophys. Res.*, *97*, 5493–5550.

Smolarkiewicz, P. K. (1983), A simple positive definite advection scheme with small implicit diffusion, *Mon. Weather Rev.*, *111*, 479–486.

Stommel, H. (1948), The westward intensification of wind-driven ocean currents, *Eos Trans. AGU*, *29*, 202–206.

von Blanckenburg, F., and H. Igel (1999), Lateral mixing and advection of reactive isotope tracers in ocean basins: Observations and mechanisms, *Earth Planet. Sci. Lett.*, *169*, 113–128.

von Blanckenburg, F., R. K. O'Nions, and J. R. Hein (1996a), Distribution and sources of pre-anthropogenic Pb isotopes in deep ocean water from Fe-Mn crusts, *Geochim. Cosmochim. Acta*, *60*, 4957–4964.

von Blanckenburg, F., R. K. O'Nions, N. S. Belshaw, A. Gibb, and J. H. Hein (1996b), Global distribution of Beryllium isotopes in deep ocean water as derived from Fe-Mn crusts, *Earth Planet. Sci. Lett.*, *141*, 213–226.

Young, W. R. (1984), The role of western boundary layers in gyre-scale ocean mixing, *J. Phys. Oceanogr.*, *14*, 478–483.

Yu, E.-F., R. Francois, and M. P. Bacon (1996), Similar rates of modern and last-glacial ocean thermohaline circulation inferred from radiochemical data, *Nature*, *379*, 689–694.